



Neuroscience

Applications Booklet





Harvard Apparatus and affiliates are cited over 232,037 times in 'Google Scholar', and over 10,000 times in 2012 alone.*

The following booklet contains examples of Harvard Apparatus products used in Neuroscience Research, along with summarizations of the experiments and related published articles.

Thank you for considering Harvard Apparatus products for your Neuroscience Research needs.

*Data compiled November 2014.



Dear Scientist,

The importance of your research work cannot be overstated. Everyone's life is impacted by a family member or friend that has a neurodegenerative disorder, a learning disability, a traumatic injury or a psychological disorder. Your work is our only hope that future generations will be relieved of such conditions. We at Harvard Apparatus congratulate and thank you for devoting your career to neuroscience research.

Harvard Apparatus and affiliated entities, have been supplying tools for neuroscience research for over 100 years. We provide researchers with an extensive product offering for animal, organ, tissue and cellular research. Whether you need to execute precise infusion into cells or animals, sample extraction, behavior analysis, or control and measure physiological parameters – Harvard Apparatus is ready to meet your needs. Our product quality, dedicated support and neuroscience expertise have made Harvard Apparatus the leader in this field. Our products have been extensively used for neuroscience experiments for decades and have been cited in thousands of publications. The enclosed is a sampling of published articles that cited the use of products from one or more of our affiliated companies. We hope that these abstracts and the bibliography at the end will assist you in your important work and that you consider Harvard Apparatus as your primary source for neuroscience research apparatus.

Application Briefs

2 - 25

Bibliography

26 - 27

Ventral Tegmental Area Neuronal Activity Correlates to Animals' Behavioral Response to Chronic Methylphenidate Recorded from Adolescent SD Male Rats

Z. Jones et al (2014)

Journal of Behavioral and Brain Science
Vol 4(4); ID 45258, 22

Introduction

Methylphenidate (MPD) is considered as the first-line pharmacotherapy to treat ADHD. More recently, MPD has also been used as a cognitive enhancement recreationally. Its therapeutic effects are not fully understood, nor are the long term effects of the drug on brain development. The ventral tegmental area (VTA) neuronal activity was recorded from freely behaving adolescent rats using a wireless recording system.

EXPERIMENT SUMMARIZATION

Materials & Methods

Male Sprague-Dawley rats (N=142_ at post natal day of about 32 days were purchased (Harlan, Indianapolis, IN, USA) and were allowed 3-4 days of acclimation in the vivarium on a 12 hour light/dark schedule prior to the electrode implantation. Food and water were given at libitum. The animals were housed individually in clear acrylic standard cages that served as both home cage and test cage for this study.

Electrodes were implanted during stereotaxic surgery on anesthetized subjects that had their heads shaved prior to the procedure. Once electrodes were implanted, subjects were allowed 3-4 days recovery in their home cages and were connected to the wireless head stage transmitter (Triangle BioSystems (TBSI); Durham, NC, USA) for acclimation for at least 2 hours/day to the behavioral and electrophysiological recording systems. At first experimental day, the animal's age was about post natal 39-41 days.

Five groups were used: saline, 0.6, 2.5, 5.0 and 10.0 mg/kg MPD. Behavioral and neuronal activity recordings were resumed for an additional hour post drug injection. The wireless TBSI head stage sent neuronal activity signals from the 4 recording electrodes to a receiver that was connected to an analog to digital converter where data was collected and stored for analysis. The experiment lasted for 10 days. On days 2 through 6, subjects received either saline or a daily MPD injection, but without neuronal recording depending on the group. On days 7 through 9, the subjects underwent a washout period in which no injections were given, and then on day 10, a saline injection was delivered. Following the saline injection on day 10, the neuronal and behavioral baseline activity was recorded for an hour followed by a rechallenge administration of either saline or MPD dose similar to day 1, and recordings were resumed for an additional hour.

Locomotor activity was recorded concomitantly with neuronal activity, using an open field activity monitoring system. The system evaluated data to horizontal activity counts, total distance travelled and the number of stereotypic movements over 10 minute bins. These bin counts were used to produce temporal graphs and histograms for total activity/hour for both the sale baseline activity and the activity after MPD administration for the experimental days 1 and 10.

Results & Conclusions

The study examined the effects of MPD on adolescent VTA neuronal firing rates and behavioral activity of freely behaving non-anesthetized SD rats. The majority of VTA neurons did not respond to acute low and medium MPD dosing (i.e 0.6 and 2.5 mg/kg MPD), while higher MPD doses of 5.0 and 10.0 mg/kg elicited mainly an increase in neuronal firing rates in response to MPD. Additional studies will need to be done in order to further understand the effects of MPD on the VTA and other brain areas of adolescent rats and how they are similar and different from adult rats. Knowledge of this will help those affected with ADHD to be better treated and will help to further comprehend the role that psychostimulants play in the brain.

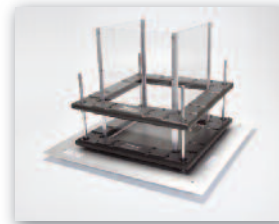


Products from TBSI used in this study:



Part #	Description
N50-4113-G3	S2W Wireless Stimulation Headset
KS-020	S2W Wireless Stimulation Accessory Kit
www.trianglebiosystems.com	

Similar locomotor activity monitoring systems used in this study:



TRU SCAN

Part #	Description
TRU SCAN	Control and Data Acquisition
L18-16XHS-10A	TRU SCAN Expander Box (for 2-10 stations)
E63-10HS	TRU SCAN Linc
U90-11	USB Interface
E63-10	TRU SCAN Arena for Mouse
E63-12	Sensor Ring for Mouse
E63-91	Elevation Rod Kit

www.coulbourn.com

Step-By-Step Instructions for Retina Recordings with Perforated Multi Electrode Arrays

Katja Reinhard, Alexandra Tikidji-Hamburyan,
Hartwig Seitter, Saad Idrees, Marion Mutter, Boris
Benkner, Thomas A. Münch

Werner Reichardt Centre for Integrative Neuroscience
and Bernstein Center for Computational
Neuroscience, University of Tübingen,
Tübingen, Germany

(2014) PLoS ONE 9:e106148

Introduction

Multi-electrode arrays are a state-of-the-art tool in retina research. The structure of the retina has allowed the use of multi-electrode arrays for high-throughput, parallel recordings of retinal responses to presented visual stimuli, and has led to significant new insights into retinal organization and function. However, using conventional arrays can be associated with three main problems: (1) low signal-to-noise ratio due to poor contact between electrodes and tissue, especially in the case of strongly curved retinas from small animals, e.g. rodents; (2) insufficient oxygen and nutrient supply to cells located on the bottom of the recording chamber; and (3) displacement of the tissue during recordings. Perforated multi-electrode arrays (pMEAs) have been found to alleviate all three issues in brain slice recordings. Over the last years, we have been using such perforated arrays to study light evoked activity in the retinas of various species including mouse, pig, and human. In this article, we provide detailed step-by-step instructions for the use of perforated MEAs to record visual responses from the retina, including spike recordings from retinal ganglion cells and in vitro electroretinograms (ERG).

EXPERIMENT SUMMARIZATION

Materials & Methods

The setup for pMEA recordings consists of two perfusion loops: An upper loop to supply the tissue with fresh solution and a lower loop to adjust the proper negative pressure. We provide an overview of this dual perfusion system and a detailed list of the components we used to build our setup.

The procedure on how to use the system is described in detail. Except for the constant vacuum pump the amplifier baseplate that allows vacuum application, and some small components, no additional material is needed compared to conventional MEA recordings. The upper perfusion system supplies the retina with fresh solution during the recordings. The lower perfusion system is only used before the experiment to fill the MEA chamber with solution without introducing air bubbles into the vacuum system. The vacuum system provides negative pressure to pull the retina towards the electrodes. This negative pressure needs to be constant to avoid fluctuations, and high enough to ensure good tissue-electrode contact without tearing the tissue. Constant negative pressure is provided by a Constant Vacuum Pump (CVP) and is further reduced by an additional fine flow control between the CVP and the MEA baseplate. The most important step for ensuring reliable negative pressure is the removal of air bubbles: any air bubble in the vacuum system will degrade the stable negative pressure. Setting up for pMEA recordings takes approximately 40–60 minutes. Except for the steps involving the vacuum system and preparation of the filter paper, all steps are very similar to conventional MEA recordings. Further, no coating of the MEA is necessary for pMEA recordings. Overall, pMEA recordings require about 10 minutes more preparation time than conventional MEAs.

Results & Conclusions

pMEAs provide good signal-to-noise ratios

The vacuum applied through the perforation of pMEAs greatly enhances the contact between the tissue and the electrodes. On good recording electrodes, we can detect

and properly spike-sort one to three cells per electrode. To get an estimate of the number of recorded cells that one might expect in such experiments, we counted the number of extractable cells in 153 recordings from mouse retina and found on average 38 ± 18 cells. Pig and human retina recordings often had even better signal-to-noise ratios and therefore lead to more sortable cells. In pig retina, we found on average 48 ± 31 cells and in human retina 51 ± 32 cells.

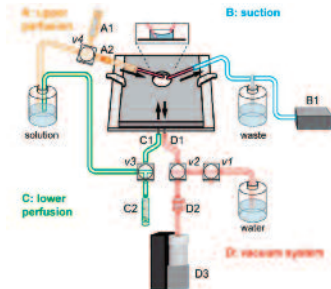
pMEAs allow stable long-term recordings

Insufficient oxygen and nutrient supply to the ganglion cell might limit the recording time. We showed various light stimuli to a mouse retina on a pMEA during 6 hours and recorded ganglion cell responses. A very simple stimulus was presented over 120 times during these 6 hours. The cell responded to every repetition of the stimulus, also after 6 hours of continuous recording.

pMEAs prevent movement of retina

We recorded ganglion cell responses to binary checkerboard stimuli to calculate receptive fields and to visualize tissue movement. Location and shape of the calculated receptive fields were very stable during an 8h recording period.

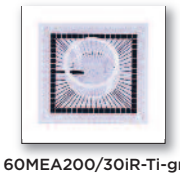
Although the preparation and adjustment of the additionally required perfusion and vacuum system might seem complicated at a first glance, the additional time required for perforated compared to conventional MEA recordings amounts to only around 10 minutes. Further, little additional material is needed when switching from standard to perforated MEA recordings. Especially when isolating single cell responses from MEA recordings, the user will appreciate the resulting high signal-to-noise ratio in pMEA recordings.



MEA setup consists of two perfusion loops. Solution is supplied to the MEA chamber from the top through the upper perfusion (A) and excessive solution is removed by the suction (B). The necessary negative pressure is supplied by the additional perfusion, consisting of the lower perfusion (C) and a vacuum (D).



Products from Multichannel Systems used in this study:



Part #	Description
MEA2100-60-System-E	MEA Recording System for one 60-electrode MEA with perfusion cannula
MEA2100-PE60/120	Perfusion Element for MEA2100-headstage
60pMEA200/30iR-Ti-gr	Perforated MEA with interelectrode distance of 200Qm, electrode diameter of 30µm, internal reference electrode and glass ring
CVP	Constant Vacuum Pump
www.multichannelsystems.com	

An immunoblot for detection of *Taenia saginata* cysticercosis

Sameh Abuseir,
Uschi Nagel-Kohl,
Sonja Wolken
& Christina Strube

Introduction

Food-borne zoonotic diseases are significant and widespread throughout the globe. It is contracted by food consumption contaminated by pathogenic organisms between species. One particular organism, *Taenia Saginata*, more commonly known as beef tapeworm is common in Africa, some parts of Eastern Europe, the Philippines, and Latin America. However, this organism is found anywhere beef is consumed. Humans are the final and bovines are the intermediate hosts to this infection. Infection with the adult *T. saginata*, or human taeniosis, is characterized by the presence of a tapeworm that is 3.5 – 20 meters long in the small intestine. Bovine cysticercosis is the infestation of the intermediate host and may suffer from cysts of *T. saginata* in their muscles and tissues. Light infestations are unlikely to be detected during meat inspections, overall there needs to be more sensitive methods for detection.

Developing an immunoblot for detection of *T. saginata* infected cattle may lead to a potential vaccine against cysticercosis and cystic echinococcosis in cattle.

EXPERIMENT SUMMARIZATION

Materials & Methods

SDS-PAGE was conducted using Hoefer Mighty Small II SE260 Mini Vertical Electrophoresis Unit in 6, 8, 10, 12, and 15% gels. 30-40µg of protein of the cyst samples were loaded per lane. Duplicate gels were done, one set was for transfer and the other set was stained with Coomassie Blue dye to visualize proteins. After electrophoresis, crude antigens from the one set of gels were transferred using the Hoefer TE22 Mighty Small Transfer Tank onto nitrocellulose membrane.

Results & Conclusions

T. saginata cyst antigen SDS-PAGE and Immunoblot

T. saginata cyst antigen showed ten visible bands ranging from 260 to 14kDa at approximately 260, 150, 130, 67 (major band), 60, 55, 50, 23, 18, and 14 kDa. All protein bands reacted with *T. saginata*-positive sera (n=10) from experimentally infected cattle. Protein bands of *T. saginata* was tested against positive *E. granulosus* sera (n=10) and showed only 18-14kDa proteins of *T. saginata* were immunoreactive. No antigenic reactions were seen with any of the extracted proteins of the tested cestodes from serum samples (n=10) of infected animals with *F. hepatica*. All negative serum samples (n=100) showed no reaction with any extracted proteins.

E. granulosus cyst antigen SDS-PAGE and Immunoblot

E. granulosus cyst antigen showed visible bands ranging from 260 to 23 kDa at approximately 260, 250, 150, 130, 120, 80, 67, 60, 55, 35, and 23kDa. All proteins bands reacted with positive *E. granulosus* sera (n=10) except for 260 and 35 kDa bands. All proteins bands reacted with positive *T. saginata* sera (n=10) except for 260, 30, and 35 kDa bands.

T. hydatigena cyst antigen SDS-PAGE and Immunoblot

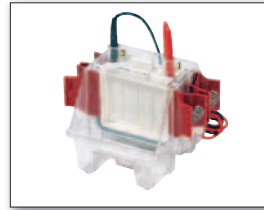
T. hydatigena cyst antigen showed visible bands ranging from 290 to 14 kDa at approximately 290, 270, 260, 150, 130, 80, 67, 55, 35, 23, and 14kDa. All proteins bands reacted with positive *T. saginata* sera (n=10) except for 290 and 14 kDa bands. All proteins bands reacted with positive *E. granulosus* sera (n=10) except for 290, 270, 260, and 14 kDa bands.

Conclusion:

There is a wide range of antigenic similarity between the different helminthes as seen in the results. This may help develop a possible vaccine against the family of Taeniidae that are affecting cattle. Two *T. saginata* protein bands were identified as potential antigens. However, substantial research on additional *Taenia* species still needs to be done to confirm results and antigen-antibody interactions.



**Products from
Hoefler
used in this study:**



Mighty Small II Mini
Vertical Electrophoresis



Mighty Small Transfer Tank

Part #	Description
SE260-10A-.75	Mighty Small II Mini Vertical Electrophoresis, Complete
SE260-10A-1.0	
SE260-10A-1.5	
TE22	Mighty Small Transfer Tank
www.hoeflerinc.com	

Implementation of a Two-dimensional Behavior Matrix to Distinguish Individuals with Differential Depression States in a Rodent Model of Depression

Jin-Young Park et al. (2014)

Exp Neurol. Sep; 23(3); 215-223

Introduction

Animal models of depression are used to study pathophysiology of depression and to advance therapeutic strategies. Stress-induced depression models in rodents are widely used. However, amenable behavior criteria and experimental procedures that are suitable for animal models have not been established. Given that depression is clinically diagnosed by multiple symptomatic criteria and stress effects are imposed to the brain non-specifically in stress-induced depression models, analyses of depression states in rodents using multiple symptomatic criteria may provide more power than any methods relying on a single symptomatic criterion.

EXPERIMENT SUMMARIZATION

Materials & Methods

Male C57BL/6 inbred mice at seven weeks of age (Eumsung, Chungbuk, Korea) were used in this investigation. Subjects were restrained for 2h daily for 14 days and depression states of individual mice were assessed using the U-field test, behavioral assessment developed to measure animal's sociability and the tail suspension test and/or forced swim test, which are the typical methods that measure psychomotor withdrawal states.

The U-field test was monitored using a computerized video tracking system (SMART, Panlab, Spain). A webcam was used to record behavioral performances in the TST and FST. Behavioral tests were performed during the light cycle (9AM-3PM). The behavior testing room was lit with indirect illumination by 20 lux for the U-field test and 250 lux for TST and FST, and sound was masked with 65 dB of white noise. Subjects were given 20 minutes to adapt to the behavior testing room prior to the start of each behavioral test.

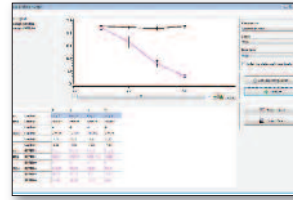
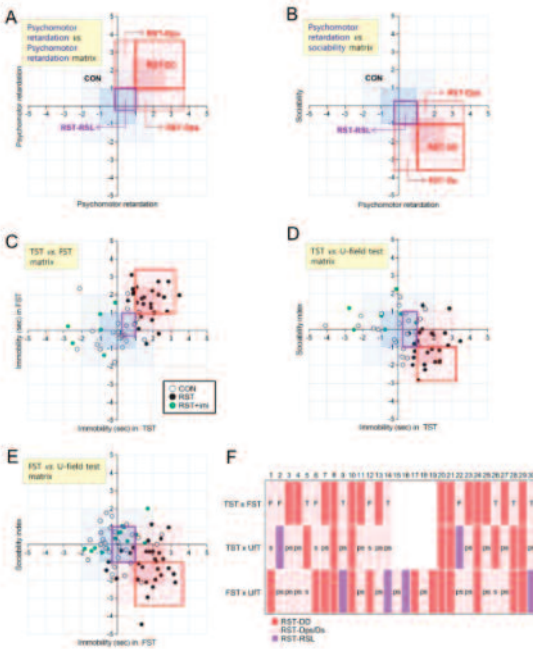
Results & Conclusions

The majority of these mice showed severe depressive behaviors in both tests, a significant proportion of them, which were all inbred mice and received the same amount of restraints, expressed differential depression states in the sociability test and psychomotor withdrawal tests. To easily readout differential depression states of individuals in two different tests, a standard method and basic parameters required to construct two-way behavior matrix were introduced.

The two-way behavioral matrix can be used not only to measure behavioral performance of a group of animals, but also to differentiate different depression states of individuals. For example, the two-way matrix differentiates behavioral states with normal sociability and psychomotor withdrawal, which was referred to as (i) RST-RSL individuals, (ii) behavioral states with normal sociability and high psychomotor withdrawal, (iii) behavioral states with low sociability and normal psychomotor withdrawal and (iv) behavioral states with low sociability and high psychomotor withdrawal, referred to "RST-DD" (Fig 3A and B) The RST-DD and

Panlab

Products from Panlab used in this study:



SMART Video Tracking Software



Cylinder for Forced Swim Test Experiments

RST-RSL individuals may have some similarity to susceptible and resilient mice, respectively, which were isolated on the basis of sociability alone [15].

Individual animals determined to be depressive by the TST and FST are not necessarily defective in psychomotor activity alone, but presumably in other symptoms as well. Similarly, individuals determined to be depressive by the U-field test are not necessarily defective in sociability alone, but presumably in other symptoms as well. Based on the same rationale, the two-way behavioral matrix may be expanded to the analyses of any two different behaviors, and should have advanced resolving power to distinguish individuals with different depression states compared with those measured by a single behavioral symptomatic criterion.

Part #	Description
76-0696	SMART Video Tracking Software
76-0471	Cylinder for Forced Swim Tests
www.panlab.com	

Protective effects of remote ischemic conditioning against ischemia/reperfusion-induced retinal injury in rats

Xuxiang Zhang et al. (2014)

Visual Neuroscience 31, 03, 246-262

Introduction

Limb remote ischemic conditioning (LRIC) provides a physiologic strategy for harnessing the body's endogenous protective capabilities against injury induced by ischemia-reperfusion in the central nervous system. This study seeks to determine if LRIC played a role in protecting the retina from ischemia-reperfusion injury. The role of astrocytes and cellular pathways was analyzed, which influence the severity of ischemia/reperfusion injury (Eng et al., 2000). Retinal ischemia promotes increased proliferation and differentiation of astrocytes. The increase in astrocyte activity following ischemia causes an increase in glial fibrillary acidic protein (GFAP) transcription and translation.

EXPERIMENT SUMMARIZATION

Materials & Methods

A total of 81 adult male Sprague-Dawley rats were randomly assigned to ischemia/reperfusion with or without remote LRIC arms. Subjects were anesthetized, orally intubated and mechanically ventilated (Rodent Ventilator Model 683, Harvard Apparatus). The retinal ischemic model was generated through right middle cerebral artery occlusion (MCAO) and pterygopalatine artery occlusion for 60 minutes followed by 1, 3, and 7 days of subsequent reperfusion.

Paraffin sections were stained to quantify the number of cells in the retinal ganglion cells (RGCs) layer throughout the duration of the study. Cellular expression of glial fibrillary acidic protein (GFAP) was detected and examined through immunohistochemistry. Protein expression was analyzed via Western blot.

Results & Conclusions

Analysis demonstrated that the loss of cells in the RGC layer were attenuated by LRIC treatment at 3 and 7 days following reperfusion ($P < 0.05$). Immunohistochemistry studies depicted a gradual increase ($P < 0.05$ in GFAP levels from day 1 through day 7 following ischemia and subsequent reperfusion, whereas LRIC reduced GFAP levels at 1, 3 and 7 days postreperfusion. The study also showed that LRIC increased the expression of Nrf2 and HO-1 at day 1 and 3 following ischemia/reperfusion.

The study concluded that limb remote ischemic conditions (LRIC) protect the rat retinal from ischemia/reperfusion injury. Although the mechanism(s) involved in retinal ischemic conditioning need to be further examined, the result of this study and current literature support the idea that the Nrf2/HO-1 pathway is directly involved in retinal protection induced by LRIC. The results exhibited may provide clues to help elucidate the protective capabilities of LRIC. The study suggests that LRIC could serve as a valuable tool for seeking therapeutics in enhancing neurological outcomes following ischemia/reperfusion injury, and suggest three directions in which therapeutics could be designed.



Products from Harvard Apparatus used in this study:



Rodent Ventilator, Model 683

Part #	Description
55-0000	Rodent Ventilator, Model 683
www.harvardapparatus.com	

Intrahippocampal glucocorticoids generated by 11 β -HSD1 affect memory in aged mice

J. Yau et al (2014)

Neurobiology of Aging
available online July 15, 2014

Introduction

Both aging and stress induce memory impairments notably in hippocampus-associated cognitive functions. Stress activates the hypothalamic-pituitary-adrenal (HPA) axis causing acute elevation of blood glucocorticoid levels, whereas in a subset of aged individuals, plasma glucocorticoid levels are elevated, and this correlates with hippocampal-associated memory deficits (Lupien et al., 1998)

In the present study, *in vivo* microdialysis was used in freely behaving mice to examine (1) the effects of aging and/or stress on intro-hippocampal CORT levels and memory during learning and retrieval; and (2) the role of 11 β -HSD1 in these processes.

EXPERIMENT SUMMARIZATION

Materials & Methods

Male mice homozygous for a targeted disruption of *hsd11b1*, congenic on the C57BL/6J genetic background and wild-type (WT) C57BL/6J mice were bred in-house under standard conditions (12 hours light-dark cycle) with food and water ad libitum until experimentation at either 6-8 months old (young) or 24-26 months old (aged) (Carter et al., 2009 and Kotelevtsev et al., 1997).

A 2-trial Y-maze task was used to assess hippocampal-dependent spatial recognition memory (Conrad et al., 1996 and Yau et al., 2011). The size of the maze allowed for *in vivo* microdialysis in freely behaving mice.

Mice were anesthetized and fixed within a stereotaxic frame for microdialysis guide implantation at a position just entering the dorsal hippocampus. Mice were allowed to recover for 4 days before microdialysis began. A CMA 7 microdialysis probe was introduced via the pre-implanted guide cannula. Subjects were individually housed in the CMA 120 system for freely moving animals with free access to food and water. The probe was perfused continuously with a sterile artificial cerebrospinal fluid at 0.3 μ l per minute using an infusion pump and samples were collected via the CMA470 Refrigerated Fraction Collector.

Histology was performed and samples were homogenized for CORT and 11 β -HSD1 activity assays.

Results & Conclusions

The study found that higher intrahippocampal CORT levels associate with impaired spatial memory retention during the behavioral tasks for the aged, WT group, but not the 11 β -HSD1 mice. Acute stress was found to elevate plasma CORT levels and impair spatial memory, and also its retrieval, in the WT, but not the 11 β -HSD1 mice. Pharmacologic inhibition of 11 β -HSD1 reduced intrahippocampal CORT levels in the aged subjects and improves spatial memory.

This study highlighted the direct role of 11 β -HSD1 in age- and stress-associated impairment of spatial memory. Evidence is presented that in aged mice as well as stressed young mice, a component part of the elevations in intra-hippocampal CORT levels during Y-maze testing is because of local 11 β -HSD1 activity and that this 11 β -HSD1 component can cause impaired spatial memory. Importantly, 11 β -HSD1 mice, that cannot reactivate hippocampal CORT and, hence amplify levels to those found in aged WT controls, resisted both the adverse effects of age and acute stress on spatial memory. Such memory effects are not a consequence of altered hippocampal MR and GR levels that do not differ between WT and 11 β -HSD1 mice (Yau et al. 2011).

Local intracellular regeneration of active glucocorticoids by 11 β -HSD1 in the hippocampus is dynamically regulated during learning. This regenerative component is even greater with aging reflecting as associated increase in 11 β -HSD1 expression in the hippocampus. The data presented that it is this rise in hippocampal CORT levels amplified by 11 β -HSD1 activity during the retrieval phase of spatial learning that appears to impair memory in aged WT controls or stressed young WT mice. Also, data suggests that when selective 11 β -HSD1 inhibitors are used to treat chronic age-related memory deficiencies, there may be the added advantage of protection from acute stress-induced memory impairments.



Products from CMA Microdialysis used in this study:



CMA 120 System



CMA 470 Refrigerated Fraction Collector

Part #	Description
CMA P000137	CMA 7 Guide Cannula
CMA P000082	CMA 7 Microdialysis Probe, 1mm length (6kDa)
CMA 8309049	CMA120 System for Freely Moving Animals
CMA 400400	CMA4004 Syringe Pump
CMA 8002770	CMA470 Refrigerated Fraction Collector
59-7316	Artificial Cerebral Spinal Fluid
www.microdialysis.com	

Similar products used in this study can be found from our other brands:

Part #	Description
76-0681	SMART Video Tracking
76-0691	SMART T/Y Maze Preconfigured Software Module
76-0079	Y-Maze
72-6335	Stereotaxic Frame, Mice and Rats

Back to basics: Comprehensive DNA quantitation using BioDrop in the UV spectrophotometry range, why is it worth it?

Boesenberg-Smith, K. A., Pessarakli, M. M. & Wolk, D. M., 2012. Assessment of DNA yield and purity: an overlooked detail of PCR troubleshooting. *Clinical Microbiology Newsletter*, 34(1), pp. 2-5.

Haque, K. A. et al., 2003. Performance of high-throughput DNA quantification methods. *BMC Biotechnology*, pp. 1-10.

Wilson, I. G., 1997. Inhibition and Facilitation of Nucleic Acid Amplification. *Applied and environmental microbiology*, October, 63(10), pp. 3741-3751.

Introduction

With the advent of new technologies aiming at more clearly discerning subtle and complex information from little amount of samples, the requirement for setting quality control processes within a particular workflow has never been greater.

Examples of areas where sample concentration determination has seemed to expand the most are proteomics and genomics which require lengthy sample preparation and data analysis steps. Set as an intermediary step, protein or nucleic acid quantitation plays a very determinant role in the outcome of many downstream experiments.

The way the quantitation is performed is equally very important: the quality control process that can potentially quantify and qualify vast amounts of sample types should be very quick and simple.

BioDrop μ Lite is a split-beam UV-Vis spectrophotometer equipped with a built-in micro-volume sample port. The micro-volume sample port is specifically designed for the quantitation of small sample volumes such as protein or nucleic acids. Set to work with as little as 0.5 μ l of sample, BioDrop μ Lite is also conceived to deliver quick and high quality measurements by setting only a single and fixed path length so as to reduce bias and inaccuracy related to path length design.

EXPERIMENT SUMMARIZATION

Materials & Methods

Sample preparation

Lyophilized pure genomic DNA sample (dsDNA) from calf thymus from Sigma (PN# D4764) was weighed with a precision scale ($d=0.1\text{mg}$) and diluted to 1000mg/ml in Tris-EDTA buffer solution pH7.4.

The master sample was subsequently diluted for constituting new samples. Each sample was vortexed and centrifuged.

The samples were measured using 1.5 μ l of solution each time. The micro-volume sample port was wiped using lint free tissue after each sample measurement

Results & Conclusions

Pure dsDNA samples diluted in Tris-EDTA buffer pH7.4 were measured using BioDrop micro-volume sample port where absorbance measurements at 260, 280 and 230nm are systematically taken. The purity ratios (A_{260}/A_{280} and A_{260}/A_{230}) were directly calculated by the BioDrop Resolution software.

The first ratio 260/280, concerns protein contamination in DNA samples. Pure DNA samples have a ratio 260/280 greater than 1.8. The samples can be equally qualified as free from proteins if the values reach 2.0 as a maximum. When protein residues are present, the ratio is shifted as an indication of the contamination.

The second ratio 260/230, concerns organic contaminant and solvents detection such as phenol, thiocyanates, urea, carbohydrates, B-mercaptoethanol and guanidinium residues from chaotropic lysis buffer which are often responsible for poor DNA detection in further DNA sequencing processes by significantly affecting the PCR reactions (Boesenberg-Smith, et al., 2012; Wilson, 1997).

If those ratios are checked against the sample concentration, within the detection range of BioDrop, a rapid estimation of the sample quality can be made. BioDrop can accurately provide purity ratio within a 1000 dynamic range for DNA samples having concentrations ranging from 2.0ng/ μ l up to 2.4 μ g/ μ l.

phone 508.893.8999 toll free 800.272.2775 fax 508.429.5732

Those above purity ratios which cannot be provided by other quantification methods must not be neglected as they add significant value to many downstream experiments in the way that known purity ratios are time saving when it comes to find the root cause of failing experiments involving, to various extents, PCR reactions. BioDrop systematically provides with the sample purity ratios when selecting any nucleic acid quantitation methods such as single stranded or double stranded DNA, RNA or oligonucleotides. Those ratios are recorded for every sample, each time a measurement is taken.

Conclusions

BioDrop micro-volume sample port measures accurate absorbance values of dsDNA samples starting from few ng/ μ l up to 2,500 ng/ μ l, covering more than a 1000 dynamic detection range.

As DNA absorbance measurement in the UV is not as straightforward as other alternative absolute quantitation methods, visualization of complementary information such as purity ratios is equally important, making this absorbance measurement method indispensable for assessing sample quality.

Because purity ratios cannot be obtained via absolute quantitation methods, BioDrop constitutes an added advantage for performing quality control of small volume samples, by providing valuable sample information over a very large concentration range.

By designing a single and unmovable path length, the path length variability over the BioDrop platform is as low as 1%, allowing accurate data comparison hence, making BioDrop very appropriate for quality control requirements of downstream experiments. As precise and accurate absorbance data are not only very valuable information for dsDNA samples, BioDrop improved fixed path length also has pre-recorded quantitation methods to measure microliter sized samples of ssDNA, RNA, oligonucleotides and proteins, allowing BioDrop to remain accurate over time, removing the need for sample port recalibration.



Products from BioDrop used in this study:



BioDrop μ LITE

Part #	Description
80-3006-51	BioDrop μ LITE
80-3006-61	BioDrop Duo
80-3006-41	BioDrop Touch
www.bio-drop.com	

Temperature-Dependent Cysteine Reactivity in the Cystic Fibrosis Transmembrane Conductance Regulator

Adapted with permission from Liu X, Dawson DC.,

Cystic fibrosis transmembrane conductance regulator: temperature-dependent cysteine reactivity suggests different stable conformers of the conduction pathway.,

Biochemistry, 50(47), 10311-7.

Copyright 2011, American Chemical Society.

Introduction

Cysteine scanning has been widely used to identify pore-lining residues in mammalian ion channels, including the cystic fibrosis transmembrane conductance regulator (CFTR). Studies of this type, however, have been typically conducted at room temperature rather than at human body temperature. Reports of substantial effects of temperature on gating and anion conduction in CFTR channels, as well as an unexpected pattern of cysteine reactivity in the sixth transmembrane segment (TM6), prompted the researchers to investigate the effect of temperature on the reactivity of cysteines engineered into TM6 of CFTR. They compared reaction rates at temperatures ranging from 22 to 37 °C for cysteines placed on either side of an apparent size-selective barrier.

The results indicate that the reactivity of cysteines to MTSES- at several positions extracellular to the position of the accessibility barrier are highly temperature-dependent. In addition, the apparent activation energy for the MTSES-/cysteine reaction exceeded that expected for diffusion or thiol-disulfide exchange in solution, as well as for CFTR gating, suggesting that the change from low to physiological temperatures is associated with a change in conformation of the outer vestibule of the pore.

These data were acquired with the aid of an OC-725 oocyte clamp amplifier, an RC-1Z imaging chamber, a CL-200 dual channel bipolar temperature controller, and an SC-20 in-line solution heater/cooler from Warner Instruments.

EXPERIMENT SUMMARIZATION

Materials & Methods

Whole Cell Recordings

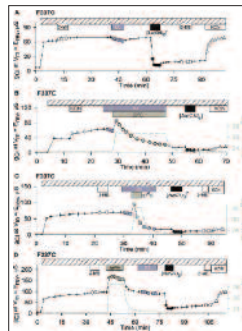
Individual oocytes were placed in a 200 mL recording chamber (RC-1Z, Warner Instruments) and continuously perfused with Frog Ringer's solution (4 mL/min). The Ringer's solution contained 98 mM NaCl, 2 mM KCl, 1 mM MgCl₂, 1.8 mM CaCl₂, and 5 mM HEPES (hemi-Na) (pH 7.4). CFTR channels were activated using 10 μM isoproterenol (a β-adrenergic agonist) and 1 mM IBMX (a phosphodiesterase inhibitor) as the stimulating cocktail (Isop+IBMX). An OC-725 amplifier (Warner Instruments) and the pClamp 8 data acquisition program (Axon Instruments) were used for whole cell recordings. Oocytes were maintained in the open circuit condition, and the membrane potential was periodically ramped from -120 to 60 mV over 1.8 s to construct the whole cell I-V plots.

Temperature Control

A dual automatic temperature controller (CL-200, Warner Instruments) and an in-line solution heater/cooler (SC-20, Warner Instruments) were used to apply acute temperature changes under a constant flow. The bath temperature was monitored. The temperature signal was digitized and recorded using a USB Data Acquisition Device (DI-158, DATAQ Instruments).

Fig. 1. Increased temperature dramatically increased the reactivity of F337C CFTR toward MTSES-. Oocytes expressing F337C CFTR were activated using a stimulatory cocktail (10 μM Isop and 1 mM IBMX, hatched bar and cross hairs) and then exposed to 1 mM 2-ME to reverse any spurious reactions of the substituted cysteine. (A) Exposure to 1 mM MTSES- (dark gray bar and circles) produced no reaction, but 1 mM [Au(CN)₂]- (black bar and circles) produced profound inhibition that was not reversed by 1 mM 2-ME but was reversed by 1 mM KCN (white bar and triangles).

(B) Increasing the temperature to 32°C in the presence of 1 mM MTSES- produced a modest reaction rate. (C) Increasing the temperature to 37°C in the presence of 1 mM MTSES- produced a rapid reaction. (D) After the oocyte had been heated to 37°C and cooled to 22°C, exposure to 1 mM MTSES- produced no evidence of a reaction.



Results & Conclusions

Representative experiments are compiled in Figure 1. These experiments illustrate the dramatic effect of increased temperature on the rate of reaction of MTSES⁻ with F₃₃₇C CFTR. In a previous study, we reported that the channel permeant probe [Au(CN)₂]⁻ reacted with a cysteine substituted at position 337 while the channel-impermeant probe MTSES⁻ did not. In many such experiments conducted at room temperature, no change in conductance was detectable upon exposure of an oocyte expressing F₃₃₇C CFTR to 1 mM MTSES⁻, even for periods exceeding 10 min.

Figure 1A depicts exposure of an oocyte expressing F₃₃₇C CFTR to MTSES⁻ at room temperature. This evoked what at first appeared to be a very slow rate of reaction, but the decline spontaneously reversed upon removal of the reagent from the superfusate. Subsequent exposure of the oocyte to the channel-permeant probe, [Au(CN)₂]⁻, produced a profound inhibition as previously reported, confirming that the cysteine thiolate remained unreacted.

Figures 1B and 1C depict experiments in which an oocyte expressing F₃₃₇C CFTR was exposed to 1 mM MTSES⁻ at 22 °C, followed by increasing the superfusate temperature to 32 or 37 °C in the presence of the mixed disulfide. Increasing the superfusate temperature in the presence of 1 mM extracellular MTSES⁻ resulted in a decrease in conductance.

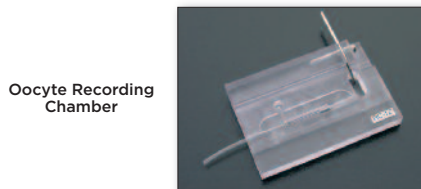
Figure 1D depicts an experiment designed to test the reversibility of the temperature-induced changes in the reactivity of a cysteine at position 337. An oocyte expressing F₃₃₇C CFTR was heated to 37 °C for 10 min and then cooled to 22 °C. The temperature excursion evoked an increase in conductance that was sustained during the period of elevated temperature but was reversed rapidly when the temperature of the superfusate was returned to 22 °C.

Conclusions

These results provide evidence of a striking temperature dependence of the reactivity of cysteines engineered into the sixth transmembrane domain (TM6) of the CFTR chloride channel toward a channel-impermeant, thiol-directed reagent. To the best of the researcher's knowledge, this is the first report comparing substituted cysteine reactivity at different temperatures, in particular, at the "physiological temperature" of 37 °C. These findings have implications for assays routinely used to test molecular models of the CFTR channel, as well as for the understanding of what structure of the pore domain is most relevant to the function of the channel in vivo.



Products from Warner Instruments used in this study:



Oocyte Recording Chamber



Oocyte Clamp Amplifier



Solution Heater/Cooler

Part #	Description	Model
64-0318	RC-1Z Oocyte Recording Chamber	RC-1Z
64-0028	OC-725C Oocyte Clamp Amplifier	OC-725C
64-1723	Dual Channel Bipolar Temperature Controller	CL-200A
64-0353	Solution Heater/Cooler, Dual Channel	SC-20
www.warneronline.com		

Dynamical modes in coupled large-scale networks

Mathias Mahn

Master Thesis, September 30, 2011,
Technion, Haifa and LMU München

Supervisors: Shimon Marom and Lars Kunz

Current address: Arison 303, Weizmann Institute of
Science, 234 Herzl Street, Rehovot 76100, Israel

mathias.mahn@weizmann.ac.il

Adopted with permission

Introduction

An aim of our group is the real-time activity analysis of compartmentalized neural networks in vitro and the reaction to the activity by electrical stimulation with a delay in the range of ms. We chose a multi-channel electrode array (MEA) based interface on which primary cortical neurons were cultured as a well-established experimental model system. These networks show a very characteristic synchronous spiking activity which is very similar to a form of network activity found in in vivo networks during development of the nervous system. To be able to perform closed loop stimulation experiments we implemented the MEA2100 system, which comprises a digital signal processor (DSP). The DSP was programmed using the MathWorks Matlab and Simulink programming framework. We present first preliminary results that are aimed at illustrating the huge space of possible investigations opened by the implementation of the MEA2100 system.

EXPERIMENT SUMMARIZATION

Materials & Methods

To be able to investigate effects of electrical coupling on separated neuronal cultures, we divided the culture chamber of 60 electrode MEAs by inserting a plastic barrier using silicone. The MEA was placed on the headstage and the aeration installed (95% air, 5 % CO₂). After placing a culture on the setup, at least 1h of spontaneous activity was recorded. To determine if the culture shows stable spiking behaviour, event detection was performed. Events were detected upon the downward crossing of a threshold set individually for each electrode to $-6 \times \text{STD}$ of the noise. Once the conditions became stable, one stimulation electrode, that efficiently evoked a network burst was chosen per compartment. The online burst detection was defined carefully. After adjusting the detection and stimulation parameters, the closed loop program was downloaded to the DSP and the coupling experiment was started. Cultures were used for experimentation for up to 60 h.

Results & Conclusions

During a closed loop experiment the voltage values from the extracellular recordings are collected and then analyzed in a chunk by the DSP. The DSP will, in case of the fulfillment of a given condition, trigger a stimulation. Here we show how fast we were able to close the loop, from the time the event happened to the time the feedback stimulus was given. The feedback stimulus was delivered with a delay of 1-2 ms. Synaptic transmission delays can range from 0.3 ms, in the extreme case of the calyx of held, to more than 5 ms. This means that the time we need to deliver a feed back is well in the physiological range of a single synaptic transmission delay. We used the separated compartment MEAs to perform several experiments, each lasting more than 36 hours. Out of these experiments we present one, which is thought to illustrate the space of possibilities, opened by the implementation of this system. In the example we present a network culture, which shows super network bursting (SNB) behaviour. This means that the network burst frequency is modulated by a slow oscillation, in

this case of about 3 to 6×10^{-3} Hz. Interestingly both compartments showed this behaviour. As a next step, the networks were electrically coupled, meaning that each detected network burst in one compartment was used to trigger a stimulation in the other compartment.

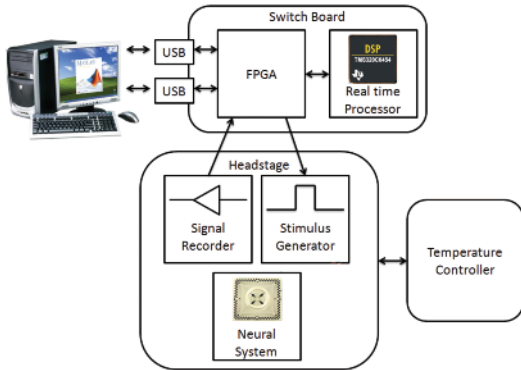


Fig 1: The setup consists of a closed-loop real-time stage that streams raw data as well as relevant data from the digital signal processor (DSP) via USB2.0 connections to a PC for visualization and archiving. In our model implementation, a 120-channel multi-electrode headstage (Multi Channel Systems MEA2100) is used to interface with a neuronal culture (Neural System). The signal recorder in the headstage digitizes the analog voltage signals from all channels after passing them through an analog 9.5 kHz low pass filter and 11 fold amplifier using the integrated analog to digital converters at 50 kHz with a resolution of 27 nV/AD. A DSP is configured to run a model, generated using MathWorks Simulink. We paced the model at 600 Qs iteration steps to process and analyze the data. Data is down-sampled to 16.7 kHz before analysis. If predefined (dynamic) conditions are met, the stimulus generator included in the headstage can be programmed online and triggered to provide a feedback stimulus after a sub-millisecond delay.

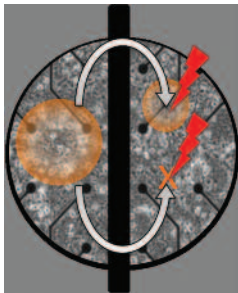


Fig 2: Network Burst Coupling Schematic. Shown is the electrical coupling procedure. Orange circle indicates a detected network burst. The lightning symbol represents a stimulation, which can either result in a network burst in the stimulated network (orange circle) or not. The black bar indicates the separation barrier between the two compartments.

multichannel*
systems

Products from Multichannel Systems used in this study:



60MEA200/30iR-Ti-gr



120MEA200/30iR-Ti-gr

Part #	Description
MEA2100-60-System	MEA Recording System for one 60-electrode MEA with perfusion cannula
60MEA200/30iR-Ti-gr or 120MEA200/30iR-Ti-gr	MEA with either 60 or 120 electrodes, interelectrode distance of 200Qm, electrode diameter of 30Qm, internal reference electrode and glass ring
www.multichannelsystems.com	

Determination of cholesterol in clinical samples

Samuel A. Roiko, Melinie A. Felmlee
and Marilyn E. Morris

Introduction

Cholesterol is the main sterol component in body tissues occurring mainly in the brain and spinal cord. Measurements in plasma help to classify hyperlipemias. Increased plasma levels are associated with atherosclerosis, nephrosis, diabetes mellitus, myxedema and obstruction jaundice. Decreased levels may occur in hyperthyroidism, anaemias, malabsorption and wasting syndromes. Normal levels are affected by stress, age, gender, hormonal balance and pregnancy. The normal range is 140-250 mg/100ml.

Use of a spectrophotometer makes cholesterol estimations very convenient, particularly for obtaining rapid results on relatively small numbers of samples, and also in non-laboratory situations. The analysis is performed directly in a cuvette at room temperature.

Provided the concentration range is 50 - 800mg/ml, foodstuff extracts can be analysed with the same method.

Cholesterol is determined at 500nm after enzymatic hydrolysis and oxidation, via the formation of the indicator quinoneimine in the presence of phenol and peroxidase.

EXPERIMENT SUMMARIZATION

Materials & Methods

Evaluation of GHB Concentration-Time Profiles in Brain Using *In Vivo* Microdialysis

The reagent can be prepared ready for use or obtained as a kit (Randox Labs. UK)

Pipette 1 ml of reagent containing:

Cholesterol esterase 0.16U/ml
Cholesterol oxidase 0.11U/ml
4-amino antipyrine 0.25 mmol/l
Phenol 25 m mol/l
Peroxidase 5.5U/ml

into each of 2 disposable cells (80-2004-53).

Libra S21/S22 operation

- Select Basic Modes (1)
- Select Concentration Select Wavelength to 500 press OK (F3)
- Enter Factor 0.533 press OK (F3)
 - The spectrophotometer can be set to read directly in concentration units (mg/100ml) using a calibration factor of 0.533 previously established experimentally.

Add 0.01ml of sample and 0.01ml water, for the blank analysis, respectively and mix.

After 10 minutes at 20-25°C:

- Insert blank cuvette. and press green run key.
 - A single blank as above suffices for subsequent analyses in the same series.
- Insert sample and press green run key

Results & Conclusions

The analysis is linear over the range 50-800 mg/100ml.

(For assays where there is no established concentration factor, calibration should be carried out using prepared standards.)

The above procedure can be easily used with other instruments in the Libra range by using the concentration mode and the 0.533 factor.



Products from Biochrom used in this study:



Part #	Description
80-2115-10	Libra S12 Visable Spectrophotomer
80-2115-25	Libra S21 Visable Spectrophotomer
80-2115-20	Libra S22 UV/Visable Spectrophotomer

The reaction can be accelerated for increased sensitivity if warmed. For this purpose the Libra S21/S22 have the following accessories:

Part #	Description
80-2109-70	8 position water heated cell changer used with an external heating bath
80-2106-04 80-2112-49	6 position Peltier heated cell changer and Temperature Control Unit
80-2106-08	Single position water heated cell holder used with an external heating bath
80-2106-12	Single position electrical cell holder, temperatures selectable from 25, 30 and 37°C
80-2106-13	Single position Peltier cell holder, temperatures select table over the whole range from 20-49°C
80-2112-25	The Sipper enables some automation of the analyses, and can be used together with a heated (not water heated) or non-heated single cell holder.

www.biochrom.co.uk

Use of Syringe Pumps for Injection into Brain Structures

Gao, M., et. al., (2007)

Functional Coupling between the Prefrontal Cortex and Dopamine Neurons in the Ventral Tegmental Area,

The Journal of Neuroscience,
27(20): 5414-5421

Introduction

Stimulation of the prefrontal cortex (PFC) has been shown to have an excitatory influence on dopamine (DA) neurons. We report here that, under nonstimulated conditions, the activity of DA neurons in the ventral tegmental area (VTA) also covaries, on a subsecond timescale, with the activity of PFC cells. Thus, in 67% of VTA DA neurons recorded in chloral hydrate-anesthetized rats, the firing of the cell displayed a slow oscillation (SO) that was highly coherent with the activity of PFC neurons. The SO was suppressed by transections immediately caudal to the PFC or by intra-PFC infusion of tetrodotoxin, suggesting that it depends on inputs derived from the PFC. Unexpectedly, the SO in most VTA DA neurons was reversed in phase relative to PFC cell activity, suggesting that at least part of PFC information is transferred to DA neurons indirectly through inhibitory relay neurons. Further understanding of this coordinated activity may provide important new insights into brain functions and disorders thought to involve both VTA DA and PFC neurons.

EXPERIMENT SUMMARIZATION

Materials & Methods

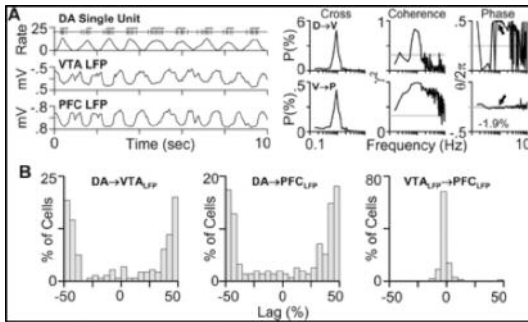
To test whether PFC inputs are involved in the generation of the SO in DA neurons, bilateral transections were made immediately caudal to the PFC to interrupt PFC inputs to DA neurons. A slit was drilled in the skull 2.0 mm anterior to bregma. The sharp pointed tip of a 3-mm-wide scalp blade was lowered to the base of skull and passed along the slit to completely interrupt connections between the PFC and the rest of the brain. Recordings commenced 30 min after the transection.

In a second group of rats, the PFC was inactivated by local infusion of TTX (Fisheries Science and Technology Development, Hebei, China). Silica capillary tubing (outer diameter, 160 μm ; inner diameter, 100 μm) was filled with TTX (10 $\text{ng}/\mu\text{l}$ in 0.9% saline) and inserted into the medial PFC (from bregma, AP, 3.0; ML, 0.7; DV, 3.5 mm). After a stable baseline recording, TTX was infused at 0.75 $\mu\text{l}/\text{min}$ for 2 min. The infusion was controlled by a Harvard Apparatus Pump 11 Elite syringe pump. Throughout the experiment, body temperature was maintained at 36-38°C with a Harvard Apparatus homoeothermic blanket system.

Effects of TTX infusion were determined by comparing recordings from the same cell before and after the infusion. Only one cell was studied in each rat. In separate groups of animals, saline (1.5 μl) was infused into the mPFC in a similar manner, or TTX (15 $\text{ng}/1.5 \mu\text{l}$) was infused into the lateral PFC (from bregma, AP, 3.0; ML, 1.4; DV, 3.5). At the end of the experiment, the injection site was verified using standard histology methods.

Results & Conclusions

Phase relationship between DA cell firing and VTA LFPs. **A**, Left, Segments of spike trains recorded from a VTA DA neuron, the corresponding rate histogram, and concurrently recorded LFPs from the VTA and PFC. Right, Cross, coherence, and phase spectra between the firing of the DA cell and VTA LFPs (D→V, top charts) and between VTA and PFC LFPs (V→P, bottom charts). As in most DA neurons, the SO in this DA cell had a nearly antiphase relationship with VTA LFPs. The latter showed a nearly in-phase relationship with PFC LFPs. **B**, Distributions of phase lags between DA cell firing and VTA LFPs (DA→V_{LFP}; left), between DA cell firing and PFC LFPs (DA→P_{LFP}; center), and between VTA and PFC LFPs (VLFP→P_{LFP}; right). y-axis values are percentages of cells that showed significant coherence with PFC or VTA LFPs.



Products from Harvard Apparatus used in this study:



Complete Homeothermic Blanket System



Pump 11 Elite

Part #	Description
50-7220F	Complete Homeothermic Blanket System with Flexible Probe
70-4505	Pump 11 Elite Infusion/Withdrawal Programmable Dual Syringe

www.harvardapparatus.com

Efficient Genome Engineering of *Toxoplasma gondii* using CRISPR/Cas9

Sidik SM, et al., (2014)

Plos One, volume 9, Issue 6, July 2014

Introduction

Toxoplasma gondii is a parasite of humans and animals, and a model for other apicomplexans including *Plasmodium* spp., the causative agents of malaria. Despite many advances, manipulating the *T. gondii* genome remains labor intensive, and is often restricted to lab-adapted strains or lines carrying mutations that enable selection. Here, the authors have used Electroporation to introduce the RNA-guided Cas9 nuclease to efficiently generate knockouts without selection, and to introduce point mutations and epitope tags into the *T. gondii* genome. These methods will streamline the functional analysis of parasite genes and enable high-throughput engineering of their genomes..

EXPERIMENT SUMMARIZATION

Materials & Methods

Transfections and Plaque Assays

Filtered *T. gondii* were washed and resuspended in Cytomix at 26108 parasites/ml. 56107 parasites were combined with 100 mg of CRISPR/Cas9 plasmid supplemented with 2 mM ATP, 5 mM GSH, and 150 mM CaCl₂, with or without 40 mg of double-stranded oligonucleotide, in a final volume of 400 ml. The CaCl₂ concentration used here matches the original formulation of Cytomix, but was added at the time of transfection to prevent the buildup of phosphate precipitates during buffer storage. Parasites were electroporated in 4 mm gap cuvettes (BTX Harvard Apparatus model no. 640) in an Electro Square Porator (BTX Harvard Apparatus). 200 parasites were added to confluent HFF monolayers in six-well dishes. In some cases, as indicated in the text, 2,000 or 20,000 parasites were used instead. If indicated, 0.2 mM Compound 2 (C₂) or vehicle (DMSO) was added to these dishes 24 hpi. All plates were allowed to incubate for a total of eight days before staining with crystal violet.

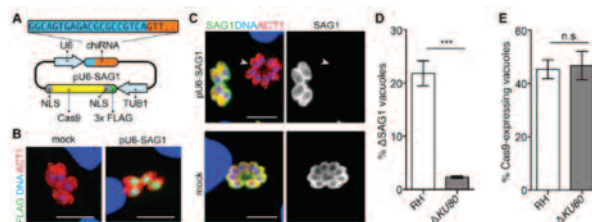


Figure 1. Targeted disruption of the SAG1 locus using CRISPR/Cas9. (A) Strategy for constructing the CRISPR/Cas9 plasmid pU6-SAG1:chiRNA encoding a protospacer specific to SAG1 (blue) and the Cas9 recognition motif (orange) was cloned under the upstream region of *T. gondii* U6. CAS9 flanked by nuclear localization signals (NLS; gray) and a FLAG tag (green) was cloned under the control of the TgTUB1 promoter. (B) Expression of Cas9 following transfection with or without pU6-SAG1. Parasites were fixed 24 hours post transfection and stained for parasite Actin (TgACT1; red), FLAG (green), and DAPI (DNA; blue). Scale bar is 10 mm. (C) Expression of SAG1 in wild-type RH parasites transfected with pU6-SAG1 Plasmid or mock-transfected parasites were allowed to grow for one lytic cycle before infecting monolayers for microscopy. Monolayers were fixed 24 hpi and stained for TgACT1 (red), SAG1 (green), and DNA. DSAG1 vacuole is indicated by an arrow. Scale bar is 10 mm. (D) Quantification of SAG1 knockout rates in RH and Δ KU80. Two-tailed Student's t-test; *** $P < 0.0005$; means \pm s.e.m., $n = 3$ experiments. (E) Quantification of transfection efficiency in the same populations 24 hours post transfection by monitoring Cas9 expression by immunofluorescence. Two-tailed Student's t-test; means \pm s.e.m., $n = 3$ experiments.

Results & Conclusions

The authors have used Electroporation to transfect *T. gondii* cells with a genome engineering method based on the CRISPR/Cas9 system that permits, with a single plasmid, the rapid and efficient disruption of genomic loci. They demonstrate that Δ KU80 parasite strains are significantly more vulnerable to these targeted disruptions than wild-type parasites, and they postulate that this vulnerability is due to the defect in this strain's ability to repair double-strand breaks using NHEJ. They further exploit the susceptibility of the Δ KU80 strain as a genetic background in which to introduce targeted point mutations and epitope tags, and show that genome editing can be achieved in 15–30% of the manipulated parasite population without the need for any form of selection. Together, these methods enhance the ability to manipulate the *T. gondii* genome and will enable highthroughput manipulation of a broad range of genetic loci.

BTX[®]

Products from BTX used in this study:

ECM 830
Generator



Part #	Description
45-0052	ECM 830 Square Wave Generator
45-0126	4 mm Cuvettes



Or use the
Gemini X2
electroporation
system

Part #	Description
452006	Gemini X2 Generator
450126	4 mm Cuvettes
www.btxonline.com	

Bibliography



Z. Jones et al (2014)

Journal of Behavioral and Brain Science
Vol 4(4); ID 45258, 22

**Katja Reinhard, Alexandra Tikidji-Hamburyan,
Hartwig Seitter, Saad Idrees, Marion Mutter, Boris
Benkner, Thomas A. Münch**

Werner Reichardt Centre for Integrative
Neuroscience and Bernstein Center for
Computational Neuroscience,
University of Tübingen,
Tübingen, Germany

(2014) PLoS ONE 9:e106148

**Sameh Abuseir,
Uschi Nagel-Kohl,
Sonja Wolken
& Christina Strube**

Jin-Young Park et al. (2014)

Exp Neurol. Sep; 23(3); 215-223

Xuxiang Zhang et al. (2014)

Visual Neuroscience 31, 03, 246-262

J. Yau et al (2014)

Neurobiology of Aging
available online July 15, 2014

Boesenberg-Smith, K. A., Pessaraki, M. M. & Wolk

D. M., 2012. Assessment of DNA yield and
purity: an overlooked detail of PCR
troubleshooting.

Clinical Microbiology Newsletter, 34(1), pp. 2-5.

Haque, K. A. et al.

2003. Performance of high-throughput DNA
quantification methods.

BMC Biotechnology, pp. 1-10.

Wilson, I. G.

1997. Inhibition and Facilitation of Nucleic
Acid Amplification.

Applied and environmental microbiology,
October, 63(10), pp. 3741-3751.

Liu X, Dawson DC.,

Cystic fibrosis transmembrane conductance
regulator: temperature-dependent cysteine
reactivity suggests different stable
conformers of the conduction pathway.,

Biochemistry, 50(47), 10311-7.

Copyright 2011, American Chemical Society.

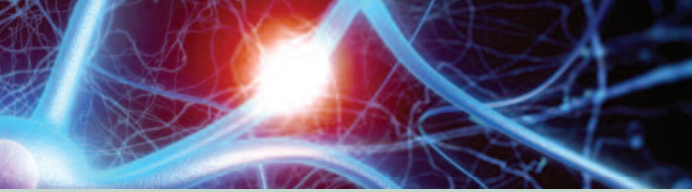
Adopted with permission

Mathias Mahn

Master Thesis, September 30, 2011,
Technion, Haifa and LMU München

Supervisors: Shimon Marom and Lars Kunz

Current address: Arison 303, Weizmann
Institute of Science, 234 Herzl Street, Rehovot
76100, Israel



Bibliography

mathias.mahn@weizmann.ac.il

Adopted with permission

**Samuel A. Roiko, Melinie A. Felmlee
and Marilyn E. Morris**

Gao, M., et al., (2007)

Functional Coupling between the Prefrontal
Cortex and Dopamine Neurons in the Ventral
Tegmental Area,

The Journal of Neuroscience,
27(20): 5414-5421

Sidik SM, et al., (2014)

Plos One, volume 9, Issue 6, July 2014



Harvard Apparatus - USA

84 October Hill Road, Holliston, MA 01746 • USA

phone **508.893.8999**
toll free **800.272.2775**
fax **508.429.5732**
email **bioscience@harvardapparatus.com**
web **www.harvardapparatus.com**



Harvard Apparatus Canada

6010 Vanden Abeele • Saint Laurent, Quebec • Canada

phone **514.335.0792**
toll free **800.361.1905**
fax **514.335.3482**
email **sales@harvardapparatus.ca**
web **www.harvardapparatus.ca**



Harvard Apparatus, S.A.R.L. - France

6 Avenue des Andes • Miniparc - Bat. 8
91952 Les Ulis Cedex • France

phone **(33) 1-64-46-00-85**
fax **(33) 1-64-46-94-38**
email **info@harvardapparatus.fr**
web **www.harvardapparatus.fr**



Harvard Apparatus Ltd/UK

22 Cambridge Science Park • Milton Road
Cambridge, CB4 0FJ • United Kingdom

phone **(44) 1732.864.001**
fax **(44) 1732.863.356**
email **sales@harvardapparatus.co.uk**
web **www.harvardapparatus.co.uk**



BTX Molecular Delivery Systems

84 October Hill Road, Holliston, MA 01746 • USA

phone **508.893.8999**
toll-free **800.272.2775**
fax **508.429.5732**
email **techsupport.btx@harvardapparatus.com**
web **www.btxonline.com**



Warner Instruments

1125 Dixwell Avenue, Hamden, CT 06514 • USA

phone **203.776.0664**
fax **203.776.1278**
email **sales@warneronline.com**
web **www.warneronline.com**



Coulbourn Instruments

5583 Roosevel Street, Whitehall, PA 18052 • USA

phone **610.395.3771** • toll free **800.424.3771**
fax **610.391.1333**
email **sales@coulbourn.com**
web **www.coulbourn.com**



HUGO SACHS ELEKTRONIK

The Physiology Specialists

Hugo Sachs Elektronik

Gruenstrasse 1 • March-Hugstetten D-79232 • Germany

phone **(49) 0 7665.92.00.0**
fax **(49) 0 7665.92.00.90**
email **info@hugo-sachs.de**
web **www.hugo-sachs.de**



Panlab S.L.U.

C/ Energia,112 • 08940 Cornellà (Barcelona) • Spain

phone **934.190.709**
fax **934.750.699**
email **info@panlab.com**
web **www.panlab.com**



CMA Microdialysis AB

Box 2 • SE-171 18 Solna • Sweden

phone **+46 8 470 10 00**
fax **+46 8 470 10 50**
email **cma@microdialysis.com**
web **www.microdialysis.com**

Harvard Apparatus & Affiliates Contact Information



Biochrom

22 Cambridge Science Park • Milton Road
Cambridge, CB4 0FJ • United Kingdom

phone **(44) 1223.423.723**
fax **(44) 1223.420.164**
email **enquiries@biochrom.co.uk**
web **www.biochrom.co.uk**



BioDrop

84 October Hill Road, Holliston, MA 01746 • USA

phone **508.893.8999**
toll free **800.272.2775**
fax **508.429.5732**
email **support@hbiosci.com**
web **www.bio-drop.com**



Hofer, Inc.

84 October Hill Road, Holliston, MA 01746 • USA

phone **508.893.8999**
toll free **800.227.4750**
fax **508.429.5732**
email **bioscience@harvardapparatus.com**
web **www.harvardapparatus.com**



Triangle BioSystems International

2224 Page Rd., Suite 108, Durham, NC 27703 • USA

phone **919.361.2663**
fax **919.544.3061**
email **sales@trianglebiosystems.com**
web **http://www.trianglebiosystems.com**



Multichannel Systems

Aspenhaustrasse 21, 72770 Reutlingen, BW • Germany

phone **+49 7121 90925 25**
fax **+49 7121 90925 11**
email **sales@multichannelsystems.com**
web **www.multichannelsystems.com**



www.harvardapparatus.com